Modelling of gas–liquid reactors — implementation of the penetration model in dynamic modelling of gas–liquid processes with the presence of a liquid bulk

Elk, E.P. van; Borman, P.C.; Kuipers, J.A.M.; Versteeg, G.F.

Published in:
Chemical Engineering Journal

ELSEVIER

Chemical Engineering Journal 76 (2000) 223–237

Chemical Engineering Journal

www.elsevier.com/locate/cej

Modelling of gas–liquid reactors — implementation of the penetration model in dynamic modelling of gas–liquid processes with the presence of a liquid bulk

E.P. van Elk [a,*], P.C. Borman [b], J.A.M. Kuipers [c], G.F. Versteeg [c]

[a] *Procede Twente BV, P.O. Box 217, 7500 AE Enschede, The Netherlands*

[b] *DSM Research, P.O. Box 18, 6160 MD Geleen, The Netherlands*

[c] *Department of Chemical Engineering, Twente University of Technology, P.O. Box 217, 7500 AE Enschede, The Netherlands*

Received 14 April 1999; received in revised form 8 November 1999; accepted 29 November 1999

Abstract

Analytical solution of models for gas–liquid reactors is restricted to a few asymptotic cases, while most numerical models make use of the physically less realistic stagnant film model. A model was developed that simulates the dynamic behaviour of gas–liquid tank reactors by simultaneously solving the Higbie penetration model for the phenomenon of mass transfer accompanied by chemical reaction and the dynamic gas and liquid phase component balances. The model makes it possible to implement an alternative for the well known Hinterland concept, which is usually used together with the stagnant film model. In contrast to many other numerical and analytical models the present model can be used for a wide range of conditions, the entire range of Hatta numbers, (semi-)batch reactors, multiple complex reactions and equilibrium reactions, components with different diffusion coefficients and also for systems with more than one gas phase component. By comparing the model results with analytical asymptotic solutions it was concluded that the model predicts the dynamic behaviour of the reactor satisfactorily. It is shown that under some circumstances substantial differences exist between the exact numerical and existing approximate results. It is also shown that for some special cases, differences can exist between the results obtained using the stagnant film model with Hinterland concept and the implementation of the Higbie penetration model.

Keywords: Gas–liquid reactors; Mass transfer; Dynamic penetration model

1. Introduction

Many chemical processes involve mass transfer of one or more gaseous components to a liquid phase in which a chemical reaction occurs. Typical examples include gas purification, oxidation, chlorination, hydrogenation [1] and hydroformylation processes.

For the selection of a reactor type it is important to classify gas–liquid transfer processes on the magnitude of the reaction-diffusion modulus (Hatta number [2]). The 'fast reactions' (Ha>2) are considered to proceed predominantly near the gas–liquid interface, while the 'slow reactions' (Ha<0.2) are considered to occur mainly in the liquid bulk. For reactions with 0.2<Ha<2, that are also frequently encountered in the chemical process industry, no distinct reaction region can be defined.

In the general case the description of a gas–liquid reactor consists of the following parts: the macro model, describing the overall gas and liquid phases, and the micro model, describing the gas–liquid interphase transport of mass and/or heat in combination with the chemical reaction.

Often applied, idealised, macro models are the plug flow (PFR) model and the ideal stirred tank (CISTR) model. Other possibilities include the plug flow with axial dispersion and the tanks in series model respectively (see [3]).

Frequently used micro models are the stagnant film model in which mass transfer is postulated to proceed via stationary molecular diffusion in a stagnant film of thickness δ [4], the penetration model in which the residence time θ of a fluid element at the interface is the characteristic parameter [5], the surface renewal model in which a probability of replacement is introduced [6] and the film-penetration model which is a two-parameter model combining the stagnant film and the penetration model [7,8].

Solution of these micro models for mass transfer accompanied by chemical reaction analytically is restricted to cases in which many simplifying assumptions are made, e.g. reaction kinetics are simple and the rate of the reaction is either very fast or very slow [9–12]. Other authors have developed approximate analytical solutions [13–16]. For all other

* Corresponding author. Tel.: +31-53-4894480/+31-53-4894337; fax: +31-53-4894774.

E-mail address: edwin.vanelk@procede.nl (E.P. van Elk).

1385-8947/00/$ – see front matter
PII: S1385-8947(99)00162-X

situations numerical techniques are required for solving the coupled mass balances.

Overall dynamic gas–liquid reactor models can be solved in two fundamentally different ways: sequential and simultaneous solution of the micro and macro model, respectively. If the penetration model is used as micro model and the gas and or liquid bulk concentrations may vary significantly during the residence time of the liquid element at the mass transfer interface (e.g. the liquid bulk is not at steady state or at equilibrium), the simultaneous strategy constitutes the only correct approach.

Due to its simplicity and relative ease of implementation in the overall gas–liquid reactor model (e.g. using a numerical analogy of the Hinterland concept [3]), the film theory is often used in numerical studies [17,18]. Both these articles deal with steady state models only. Romainen and Salmi [19,20] have published a paper in which a dynamic film-penetration theory is adopted.

The film theory and Hinterland concept can, in many cases be applied successful. However, the penetration model and the surface renewal model are to our opinion preferred since they are physically more realistic models [3,21]. Since it is not possible to implement the Hinterland analogy directly for these models, a dynamic reactor model is required that uses a somewhat different approach. Until now no such model has been published in literature.

In this paper, a dynamic gas–liquid reactor model is presented which simultaneously solves the Higbie penetration model and an instationary CISTR for the gas and the liquid phase, respectively. The model is suited for the phenomenon mass transfer with complex (ir)reversible chemical reaction(s) and is valid for the entire range of Hatta numbers. This paper concentrates on describing and validating the model. A more practical application of the model for analysing the dynamics of gas–liquid processes is given elsewhere [22].

2. Theory

2.1. Introduction

The problem considered is a dynamic gas–liquid reactor with mass transfer followed by an (ir)reversible chemical reaction of general order with respect to both reactants and products:

$$\mathrm{A(g)} + \gamma_\mathrm{b}\mathrm{B(l)} \rightleftarrows \gamma_\mathrm{c}\mathrm{C(l)} + \gamma_\mathrm{d}\mathrm{D(l)} \tag{1}$$

with the following overall reaction rate equation:

$$R_\mathrm{a} = k_{R,m,n,p,q}[\mathrm{A}]^m[\mathrm{B}]^n[\mathrm{C}]^p[\mathrm{D}]^q - k_{R,r,s,t,v}[\mathrm{A}]^r[\mathrm{B}]^s[\mathrm{C}]^t[\mathrm{D}]^v \tag{2}$$

The reaction rate expression is based on order-kinetics. If p, q, r and s are zero, a reversible 1,1-reaction is obtained. An irreversible 1,1-reaction is obtained by putting $k_{R,r,s,t,v}$ to zero. Other reactions, including multiple (in)dependent reactions, or other kinetics, like Langmuir–Hinshelwood, can easily be included in the present model. For simplicity reasons only one reaction and only one gas phase component is considered in the current work. Also for simplicity reasons, isothermal models were assumed, the temperature can however be implemented as additional component via implementation of the energy balance.

The mass transfer in the gas phase is described with the stagnant film model while for the liquid phase the penetration model is used. Further postulations in the actual dynamic reactor model are: (1) both the gas and the liquid bulk can be assumed to be a CISTR; (2) the reaction only takes place in the liquid phase; (3) the contact time is substantially smaller than the liquid phase residence time.

2.2. Micro model

For the penetration model the balances for each species for the phenomenon mass transfer followed by a chemical reaction yields the following set of equations:

$$\frac{\partial[\mathrm{A}]}{\partial t} = D_\mathrm{a}\frac{\partial^2[\mathrm{A}]}{\partial x^2} - R_\mathrm{a} \tag{3}$$

$$\frac{\partial[\mathrm{B}]}{\partial t} = D_\mathrm{b}\frac{\partial^2[\mathrm{B}]}{\partial x^2} - \gamma_\mathrm{b}R_\mathrm{a} \tag{4}$$

$$\frac{\partial[\mathrm{C}]}{\partial t} = D_\mathrm{c}\frac{\partial^2[\mathrm{C}]}{\partial x^2} + \gamma_\mathrm{c}R_\mathrm{a} \tag{5}$$

$$\frac{\partial[\mathrm{D}]}{\partial t} = D_\mathrm{d}\frac{\partial^2[\mathrm{D}]}{\partial x^2} + \gamma_\mathrm{d}R_\mathrm{a} \tag{6}$$

To be solved uniquely the four non-linear partial differential equations (3)–(6) require one initial and two boundary conditions, respectively. The initial condition is given by

$$t = 0 \text{ and } x \geq 0, \quad [\mathrm{A}] = [\mathrm{A}]_{\mathrm{l,bulk}}, \quad [\mathrm{B}] = [\mathrm{B}]_{\mathrm{l,bulk}}, \quad [\mathrm{C}] = [\mathrm{C}]_{\mathrm{l,bulk}}, \quad [\mathrm{D}] = [\mathrm{D}]_{\mathrm{l,bulk}} \tag{7}$$

The boundary condition for $x=\delta_\mathrm{p}$ is given by

$$t > 0 \text{ and } x = \delta_\mathrm{p}, \quad [\mathrm{A}] = [\mathrm{A}]_{\mathrm{l,bulk}}, \quad [\mathrm{B}] = [\mathrm{B}]_{\mathrm{l,bulk}}, \quad [\mathrm{C}] = [\mathrm{C}]_{\mathrm{l,bulk}}, \quad [\mathrm{D}] = [\mathrm{D}]_{\mathrm{l,bulk}} \tag{8}$$

where the thickness δ_p of the liquid element is assumed to be infinite with respect to the penetration depth of the gas phase component. The concentrations of the liquid bulk used in Eqs. (7) and (8) follow from the macro model for the liquid bulk.

The second associated boundary condition is obtained by assuming that the species B, C and D are non-volatile and that the flux of component A from the gas phase is equal to the flux of component A to the liquid phase. The use of the latter assumption instead of assuming that $[\mathrm{A}]=[\mathrm{A}]_{\mathrm{l},i}$ at $x=0$ is convenient in view of the applicability of the model

for cases where a part of the resistance against mass transfer is situated in the gas phase:

$$-D_a\left(\frac{\partial[A]}{\partial x}\right)_{x=0} = k_g([A]_{g,bulk} - [A]_{g,i}),$$
$$\left(\frac{\partial[B]}{\partial x}\right)_{x=0} = \left(\frac{\partial[C]}{\partial x}\right)_{x=0} = \left(\frac{\partial[D]}{\partial x}\right)_{x=0} = 0 \quad (9)$$

2.3. Macro model

The generally applicable material balance of a component in a certain phase in a tank reactor is:

$$\begin{array}{lcll} \langle\text{accumulated}\rangle & = & + & \langle\text{reactor feed}\rangle \\ & & - & \langle\text{reactor outlet}\rangle \\ & & + & \langle\text{interfacial mass transfer}\rangle \\ & & + & \langle\text{reaction in the bulk phase}\rangle \end{array} \quad (10)$$

For the gas phase only component A has to be considered:

$$\varepsilon_g V_R \frac{d[A]_g}{dt} = \Phi_{g,in}[A]_{g,in} - \Phi_{g,out}[A]_g - J_a a V_R \quad (11)$$

The liquid phase bulk component balances are given by

$$\varepsilon_l V_R \frac{d[A]_l}{dt} = \Phi_{l,in}[A]_{l,in} - \Phi_{l,out}[A]_l + J_a a V_R - R_a \varepsilon_l V_R \quad (12)$$

$$\varepsilon_l V_R \frac{d[B]_l}{dt} = \Phi_{l,in}[B]_{l,in} - \Phi_{l,out}[B]_l - \gamma_b R_a \varepsilon_l V_R \quad (13)$$

$$\varepsilon_l V_R \frac{d[C]_l}{dt} = \Phi_{l,in}[C]_{l,in} - \Phi_{l,out}[C]_l + \gamma_c R_a \varepsilon_l V_R \quad (14)$$

$$\varepsilon_l V_R \frac{d[D]_l}{dt} = \Phi_{l,in}[D]_{l,in} - \Phi_{l,out}[D]_l + \gamma_d R_a \varepsilon_l V_R \quad (15)$$

where the mass transfer flux, J_a, is defined as:

$$J_a = (k_{ov})_{k_g,k_l,E_a,m_a}(m_a[A]_{g,bulk} - [A]_{l,bulk}) \quad (16)$$

To solve the differential equations (11)–(15) uniquely, they require an initial condition

$$t = 0, \quad [A]_g = [A]_g^0, \quad [A]_l = [A]_l^0,$$
$$[B]_l = [B]_l^0, \quad [C]_l = [C]_l^0, \quad [D]_l = [D]_l^0 \quad (17)$$

2.4. Overall reactor model

In literature [23,24] it is sometimes asserted that the macro model can be implemented as boundary conditions for the micro model. For the penetration model, however, this is not straightforward in case that the liquid phase bulk concentrations may vary significantly during the contact time. This situation occurs when the liquid phase is not at equilibrium and/or in case of (ir)reversible reactions when Ha<2.

According to the penetration model a liquid element is exposed at the gas–liquid interface for a period θ during which mass transfer takes place. Next, the element is mixed up with the liquid bulk and replaced by a new fresh one. The dimensions of the liquid element are assumed to be infinite compared to the penetration depth and therefore no direct mass transport to the liquid bulk via the liquid element occurs.

The mixing with the liquid bulk must be taken into account instantaneously after the contact time θ. It has been assumed that the contact time is much smaller than the liquid phase residence time. Therefore the convection may also be taken into account instantaneously. The liquid phase concentration after these contributions is thus given by (i=A, B, C, D)

$$[i]_l = \frac{N_{i,elem} + N_{i,bulk} + (\Phi_{l,in}[i]_{l,in} - \Phi_{l,out}[i]_{l,out})\theta}{\varepsilon_l V_R} \quad (18)$$

where the first two terms of the numerator present the number of moles present in the total liquid phase after the contact time (see Fig. 1)

$$N_{i,elem} + N_{i,bulk} = [i]_{bulk}\varepsilon_l V_R + \int_0^{\delta_p} ([i] - [i]_{bulk})\, dx\, a V_R \quad (19)$$

and the last two terms of the numerator of Eq. (18) present the convection in the liquid phase.

The macro model Eqs. (11)–(15) to be used as boundary conditions for the micro model need to be simplified to

$$\frac{d[A]_{g,bulk}}{dt} = \frac{[A]_{g,in}}{\tau_{g,in}} - \frac{[A]_{g,bulk}}{\tau_{g,out}} - \frac{J_a a}{\varepsilon_g} \quad (20)$$

$$\frac{d[A]_{l,bulk}}{dt} = -R_{a,bulk} \quad (21)$$

$$\frac{d[B]_{l,bulk}}{dt} = -\gamma_b R_{a,bulk} \quad (22)$$

$$\frac{d[C]_{l,bulk}}{dt} = \gamma_c R_{a,bulk} \quad (23)$$

$$\frac{d[D]_{l,bulk}}{dt} = \gamma_d R_{a,bulk} \quad (24)$$

where the mass transfer flux, J_a, is being derived from boundary condition (9) of the micro model

$$J_a = -D_a\left(\frac{\partial[A]}{\partial x}\right)_{x=0} = k_g\left([A]_{g,bulk} - \frac{[A]_{x=0}}{m_a}\right) \quad (25)$$

The Eqs. (20)–(24) are only valid provided that the mass transfer and the convection terms that have been left out are processed instantaneously according to Eq. (18) after each contact time θ.

The solution of the overall reactor model thus proceeds in three steps, where N=1 at the start (see Fig. 1): (1) the micro model (Eqs. (3)–(9)) and the simplified macro model (Eqs. (20)–(25)) are solved simultaneously from $t=(N-1)\theta$ to $t=N\theta$; (2) at $t=N\theta$ the liquid element is mixed up with the liquid bulk instantaneously using Eqs. (18) and (19); (3) N is increased by one and the process is repeated for the next period θ. Therefore the overall reactor model produces a result after each contact period.

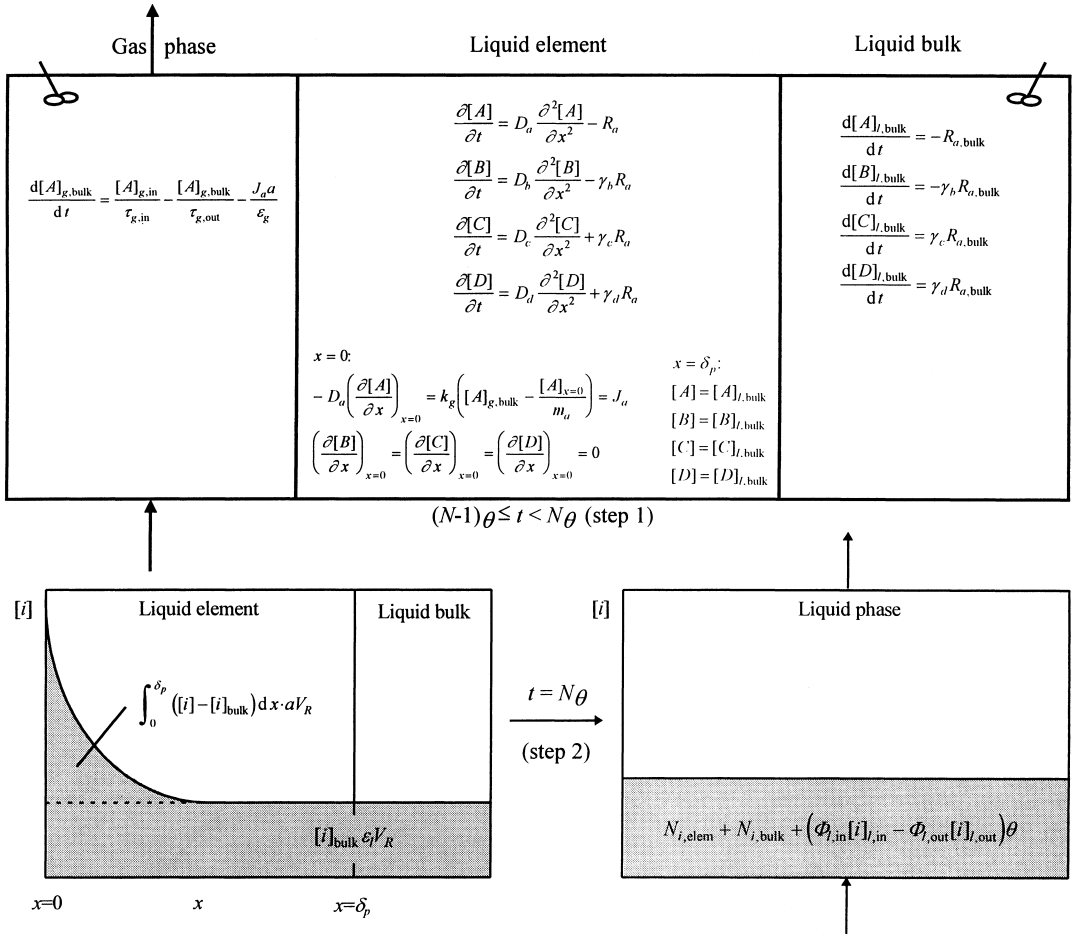

Fig. 1. The overall reactor model.

2.5. Enhancement factor and utilisation factor

The enhancement factor, E_a, defined as the ratio of the mass flux of component A through the interface with chemical reaction and driving force ($[A]_{l,i} - [A]_{l,bulk}$) to the mass flux through the interface without chemical reaction, but with the same driving force, can be obtained from the calculated concentration profiles. If gas phase mass transfer resistance can be neglected (i.e. $[A]_{g,bulk} = [A]_{g,i}$) the enhancement factor, E_a, is estimated by

$$E_a \equiv \frac{J_{a,\text{with reaction}}}{J_{a,\text{without reaction}}} \approx \frac{(1/\theta)\int_{(N-1)\theta}^{N\theta} - D_a(d[A]/dx)_{x=0}\,dt}{(1/\theta)\int_{(N-1)\theta}^{N\theta} k_l([A]_{l,i} - [A]_{l,bulk})\,dt} \quad (26)$$

For slow reactions (Ha<0.2), the influence of the reaction in the liquid bulk has a significant effect, but since the enhancement factor is always 1.0 for slow reactions it supplies no additional information.

Therefore two additional dimensionless parameters are used: the degree of saturation and the degree of utilisation of the liquid bulk. The degree of saturation of the liquid bulk is the ratio of the liquid phase concentration of A to the liquid phase concentration of A when the liquid phase is saturated

$$\eta_a \equiv \frac{[A]_{l,bulk}}{[A]_{l,sat}} \approx \frac{[A]_{l,bulk}}{m_a[A]_g} \quad (27)$$

For increasing reaction rate or decreasing mass transfer rate the degree of saturation will approach to a certain minimum (often zero) and for decreasing reaction rate or increasing mass transfer rate the degree of saturation will approach a certain maximum.

The degree of utilisation of the liquid phase is the ratio of the actual conversion rate of A to the conversion rate of A that would occur if the entire reaction phase were in equilibrium with the interface

$$\eta \approx \frac{(1/\theta)\int_{(N-1)\theta}^{N\theta} \xi_a\,dt}{\int_{(N-1)\theta}^{N\theta} R_{a,sat}\,dt\,\varepsilon_l V_R} \quad (28)$$

For increasing reaction rate or decreasing mass transfer rate the degree of utilisation will approach to a certain minimum (often zero) and for decreasing reaction rate or increasing

mass transfer rate the degree of utilisation will approach to a certain maximum.

3. Numerical treatment

In the penetration model, the concentration profiles are time-dependent: they develop a solution of a system of coupled non-linear parabolic partial differential equations subject to specified initial and two point boundary conditions. The approach used to solve these models is based on the method presented by Versteeg et al. [23], however, in the discretisation scheme two additional gridlines are introduced for the ordinary differential equations of the macro model that have to be solved simultaneously.

The implicit discretisation method used is known as the Baker and Oliphant [25] discretisation. For the time derivative a three-point backward discretisation is used (with superscript j indicating the time level) leading to (i=A, B, C, D)

$$\frac{\partial [i]}{\partial t} \rightarrow \frac{3[i]^{j+1} - 4[i]^{j} + [i]^{j-1}}{2\Delta t} \tag{29}$$

The finite difference form of the reactor model thus leads to relations between concentrations in five grid points for the micro model, four grid points for the gas phase macro model and three grid points for the liquid phase macro model, clustered as 'molecules' as shown in Fig. 2. Only for j=0 these molecules are not possible, because no grid points with time index −1 exist. Therefore in the first step, a two-point backward discretisation (Euler) is used at the cost of lower order truncation error.

The integrals of Eqs. (19), (26) and (28) are calculated using the Simpson's 1/3 rule.

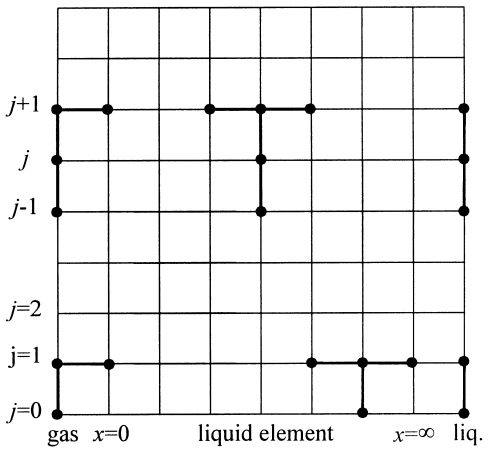

Fig. 2. Discretisation scheme.

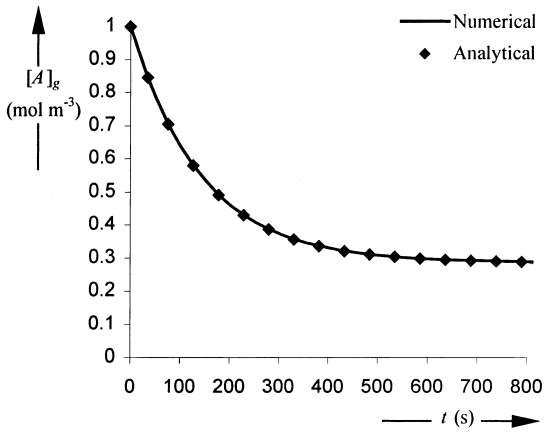

Fig. 3. Development of the component concentrations in the reactor during Case 1.

4. Validation results

4.1. Introduction

In order to validate the model, runs of the numerical solution method have been carried out on three fictitious cases. The numerical solutions are compared with analytical solutions to check the validity of the numerical method used. The cases are fictitious, and chosen so that, using physically realistic data, all relevant limit cases are tested. Emphasis is put on validation of the micro model, since this is the most complex part of the overall reactor model. Validation of the macro model is shown in Figs. 3, 5 and 8. The cases are:

1. physical absorption: A(g) → A(l) with a dynamic gas phase and a static liquid phase,
2. absorption and equilibrium reaction: A(g) → A(l), A(l) + B(l) ⇄ C(l) + D(l) and $R_a = k_{1,1}[A][B] - k_{-1,-1}[C][D]$ in a batch reactor,
3. absorption accompanied by first-order irreversible chemical reaction: A(g) → A(l), A(l) → P(l) with $R_a = k_1[A]$. This case is compared with the analytical solution of the film model.

4.2. Physical absorption

The first simulation was carried out to check that the dynamic gas phase macro model (Eq. (20)) was correctly implemented in the previously tested [23] micro model. The simulation is described in Table 1.

The results of Case 1 are presented in Fig. 3. It can be seen that the numerical solution coincides with the analytical solution. Studying the profiles in the liquid element in Fig. 4 it can be concluded that the decrease of the concentration at x=0 corresponds to the decrease of the gas phase concentrations. This is achieved by the implementation of the gas phase macro model as boundary condition of the micro model.

Table 1
Parameters used in Case 1

Case	$A(g) \rightarrow A(l)$
$[A]_{g,in}$	$1\,mol\,m^{-3}$
$[A]_g^0$ (initial state)	$1\,mol\,m^{-3}$
$[A]_l$ (fixed)	$0\,mol\,m^{-3}$
k_l	$5\times10^{-5}\,m\,s^{-1}$
k_g	$100\,m\,s^{-1}$ (no gas resistance)
D_a	$10^{-9}\,m^2\,s^{-1}$
m_a	0.5
V_R	$10\,m^3$
ε_g	0.5
a	$100\,m^2\,m^{-3}$
$\Phi_{g,in/out}$	$0.01\,m^3\,s^{-1}$
θ	0.51 s

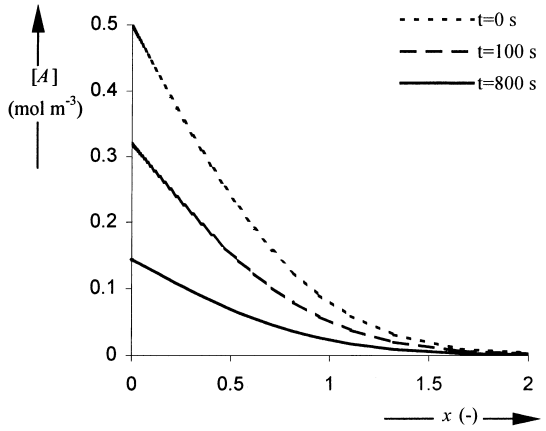

Fig. 4. Concentration profiles in the liquid element at the end of a contact period at different times during Case 1.

4.3. Equilibrium reaction in a batch reactor

The second case (Table 2) was carried out to check that the chemical reaction and the dynamic liquid phase macro model (Eqs. (18)–(24)) were correctly implemented in the model. A reversible reaction in a batch reactor was chosen so that the analytical steady state solution is known: the chemical reaction will be at equilibrium ($k_{1,1}/k_{-1,-1}=[C]_l[D]_l/[A]_l[B]_l$) and the gas and liquid phases will also be at equilibrium ($[A]_l=m_a[A]_g$).

Table 2
Parameters used in Case 2

Case (batch reactor)	$A(g) \rightarrow A(l)$, $A(l)+B(l) \rightleftarrows C(l)+D(l)$; $R_a=k_{R,1,1}[A][B]-k_{R,-1,-1}[C][D]$
$k_{R,1,1}$	$10\,m^6\,mol^{-2}\,s^{-1}$
$k_{R,-1,-1}$	$1\,m^6\,mol^{-2}\,s^{-1}$
$[A]_g^0$ (initial state)	$1\,mol\,m^{-3}$
$[B]_l^0$ (initial state)	$1\,mol\,m^{-3}$
$[A, C, D]_l^0$ (initial state)	$0\,mol\,m^{-3}$
k_l	$5\times10^{-5}\,m\,s^{-1}$
k_g	$100\,m\,s^{-1}$ (no gas resistance)
D_i	$10^{-9}\,m^2\,s^{-1}$
m_a	0.5
V_R	$10\,m^3$
ε_g	0.5
a	$100\,m^2\,m^{-3}$
θ	0.51 s

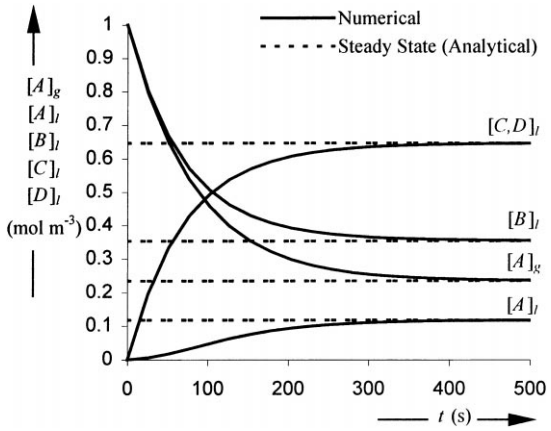

Fig. 5. Development of the component concentrations in the reactor during Case 2.

The results of Case 2 are presented in Fig. 5. The numerical results approach and achieve the analytical steady state solution.

From the profiles in the liquid element (Fig. 6) it can be seen that at the beginning component B is consumed within the liquid element and products C and D are produced. Near the gas–liquid interface, where the concentration of A has the highest value the reaction rate is fastest and the consumption of component B is maximum. Once the stationary state is achieved (t>500) the concentration of all components remain constant over the entire liquid element. The reaction is at equilibrium and there is no net gas–liquid mass transfer.

4.4. Absorption and irreversible 1,0-reaction

For the third case there is no real analytical solution of the penetration model available. Therefore, a comparison has been made between the numerical model and the analytical

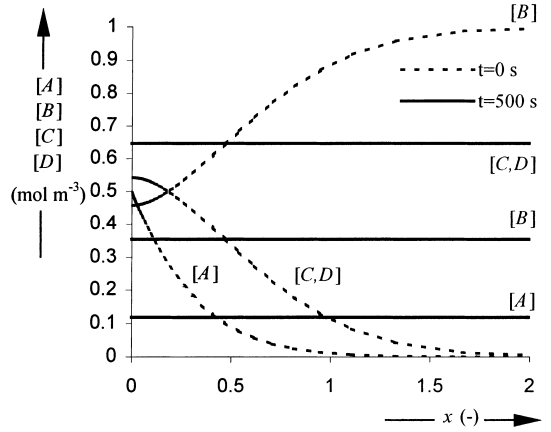

Fig. 6. Concentration profiles in the liquid element at the end of a contact period at different times during Case 2.

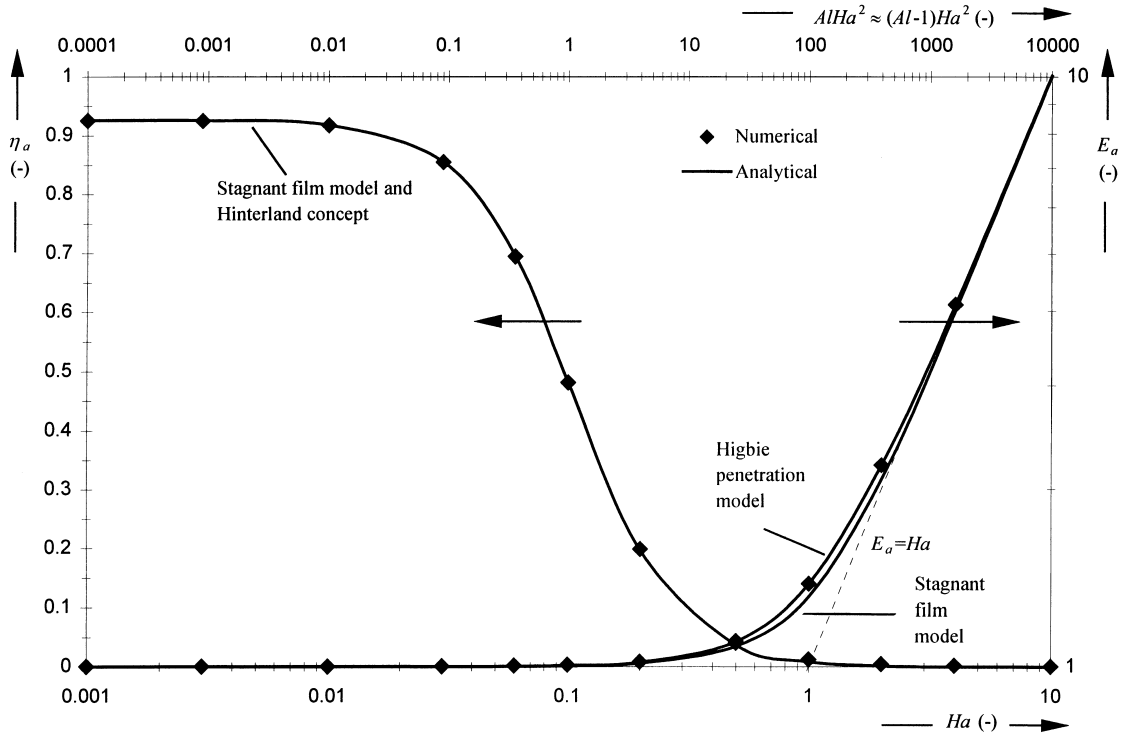

Fig. 7. Comparing analytical (Hinterland concept) and numerical (80 gridpoints) results of saturation and enhancement factors under steady state conditions of Case 3.

solution of the film model using the Hinterland concept [3]. Both solutions must result in similar, but not necessarily equal results. The conditions for the simulation are described in Table 3. Fig. 7 and Table 4 give the steady state results of the saturation (left axis) and the enhancement factor (right axis) as a function of both the Hatta number and the value of $(Al-1)Ha^2$, where the Hinterland ratio Al is defined as the ratio between the total reaction phase volume and the reaction phase film volume

Table 3
Parameters used in Case 3

Case	A(g) → A(l), A(l) → P(l); $R_a=k_{R,1,0}[A]$
$k_{R,1}$	$2.5\times10^{-6}\leq k_{R,1}\leq250$
	$0.001\leq Ha\leq10$
$[A]_{g,in}$	$1\,mol\,m^{-3}$
$[i]_{l,in}$	$0\,mol\,m^{-3}$
$[A]_g^0$ (initial state)	$1\,mol\,m^{-3}$
$[P]_l^0$ (initial state)	$0\,mol\,m^{-3}$
$[A]_l^0$(initial state)	$0\,mol\,m^{-3}$
k_l	$5\times10^{-5}\,m\,s^{-1}$
k_g	$100\,m\,s^{-1}$ (no gas resistance)
D_i	$10^{-9}\,m^2\,s^{-1}$
m_a	0.5
V_R	$10\,m^3$
ε_g	0.5
a	$250\,m^2\,m^{-3}$
$\Phi_{g,in/out}$	$0.01\,m^3\,s^{-1}$
$\Phi_{l,in/out}$	$0.01\,m^3\,s^{-1}$
θ	0.51 s

Table 4
Comparing analytical and numerical results (80 gridpoints) of saturation and enhancement factors under steady state conditions of Case 3

Ha	$Al\,Ha^2$	$E_{a,an,pen}$	$E_{a,num}$	$\eta_{a,an,film}$	$\eta_{a,num}$
0.001	0.0001	1.000	1.001	0.926	0.925
0.003	0.0009	1.000	1.001	0.925	0.925
0.01	0.01	1.000	1.002	0.917	0.917
0.03	0.09	1.000	1.003	0.855	0.855
0.06	0.36	1.002	1.005	0.695	0.695
0.1	1	1.004	1.008	0.482	0.481
0.2	4	1.017	1.020	0.197	0.198
0.5	25	1.103	1.106	0.037	0.040
1	100	1.379	1.381	0.008	0.012
2	400	2.196	2.199	0.001	0.005
4	1600	4.098	4.102	0.000	0.002
10	10000	10.04	10.05	0.000	0.001

$$Al = \frac{\varepsilon_l}{a\delta} = \frac{\varepsilon_l k_l}{a D_a} \tag{30}$$

The physical meaning of $(Al-1)Ha^2$ is the ratio of the maximum conversion in the liquid bulk to the maximum transport through the film.

The analytical solutions shown in Fig. 7 can be found in the book of Westerterp et al. [3]. Several conclusions can be drawn from the figure:

1. For this case the numerical calculated saturation coincides the analytical solution of the film model with Hinterland concept.

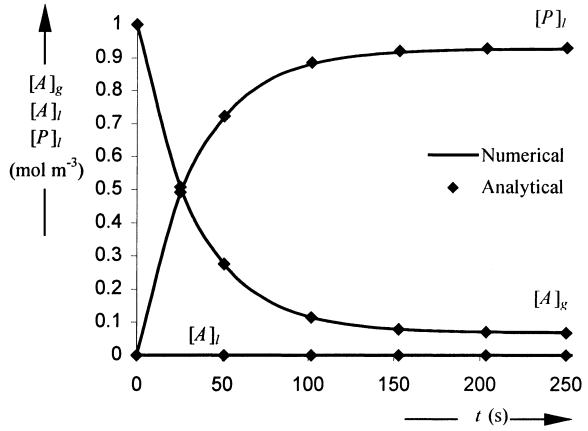

Fig. 8. Development of the component concentrations in the reactor during Case 3.

2. The numerical calculated enhancement factors coincide with the analytical solution of the penetration model.
3. For Ha<0.2 (slow reactions) the enhancement factor equals unity for all values of $(Al-1)Ha^2$. The mass transfer is not enhanced. In that case the saturation is an important parameter.
4. For Ha > 2.0 (fast reaction) the enhancement factor equals the Hatta number. The mass transfer is enhanced by the reaction.
5. For $(Al-1)Ha^2 \ll 1$ the saturation reaches an upper limit.
6. For $(Al-1)Ha^2 \gg 1$ the saturation goes to zero. In that case the enhancement factor is an important parameter.

From Table 4 it can be concluded that the analytical and the numerical solutions are similar, although a small discrepancy is found between the saturation factors at large Hatta numbers (Ha > 0.2). This is discussed in more detail in Section 5.2.

For Ha > 2.0, a dynamic analytical solution is also available. The development of the concentrations in time for Case 3 is shown in Fig. 8 for Ha=2.0. Fig. 8 demonstrates that the dynamic solution obtained analytically gives exactly the same results as the numerical solution obtained using the presented model.

5. Applications

5.1. Introduction

In the previous section the numerical results of the model were validated by comparison with exact, analytical solutions. This section discusses cases for which only approximate analytical or no solutions at all are available. Again, all data used is fictitious and chosen so that some interesting phenomena can be stressed.

It is shown that under certain defined conditions substantial deviations exist between the exact numerical and the approximate analytical results. It is also demonstrated that pronounced differences can occur between the stagnant film model with Hinterland concept [3] and application of the Higbie penetration model.

The applications discussed here concentrate on micro scale parameters (concentration profiles) and steady state results (degree of utilisation and saturation). Application of the model on macro scale parameters (dynamics of concentration and temperature at the reactor outlet) are discussed elsewhere [22].

5.2. Absorption and irreversible 1,0-reaction

Additional simulations were performed for Case 3, varying the specific contact area a from 2.5 to 2500 m^{-1}. The steady state results are shown in Fig. 9 together with the analytical solution of the stagnant film model with Hinterland concept.

For a specific contact area of 2.5, 25 and 250 m^{-1} the solution of the stagnant film model seems to coincide the solution of the penetration theory. However, at a specific higher contact areas, e.g. 2500 m^{-1}, there is a substantial discrepancy between the solutions of both the models. The penetration theory predicts substantial larger liquid phase concentrations for Ha > 0.2 than predicted by the film model with Hinterland concept. For Ha<0.2 no discrepancy is found.

The reason for this discrepancy is that the film model with Hinterland concept assumes a stagnant film, not being part of the liquid bulk, whereas the penetration model assumes liquid elements that are mixed up with the liquid bulk after each contact time. Therefore, the species present inside the liquid element are considered as part of the liquid phase and for specific conditions this results in a larger liquid phase concentration.

For processes controlled by the rate of the kinetics (Ha<0.2), these two different methods give equal results because most species are present inside the liquid bulk and the excess of species present in the liquid element (the last term of Eq. (19)) can be neglected. For processes controlled completely or partly by the rate of the mass transfer (Ha > 0.2), these two different methods give different results because the excess of species present in the liquid element (the last term of Eq. (19)) can no longer be neglected compared to the total amount of species present in the liquid phase (Eq. (19)).

The above mentioned explanation means that the discrepancy must exist for all situations where Ha > 0.2, independent of the specific contact area a. How to explain that in Fig. 9 a discrepancy is only visible for a=2500 m^{-1}? This is because of the scale of the y-axis in Fig. 9. The cases for specific contact areas of 2.5, 25 and 250 m^{-1} have the same discrepancies between the film model with Hinterland concept and the presented implementation of the penetration theory, but the differences are not visible because of the scale of the y-axis. From Table 5 it is clear that there is a discrepancy for all cases once Ha > 0.2.

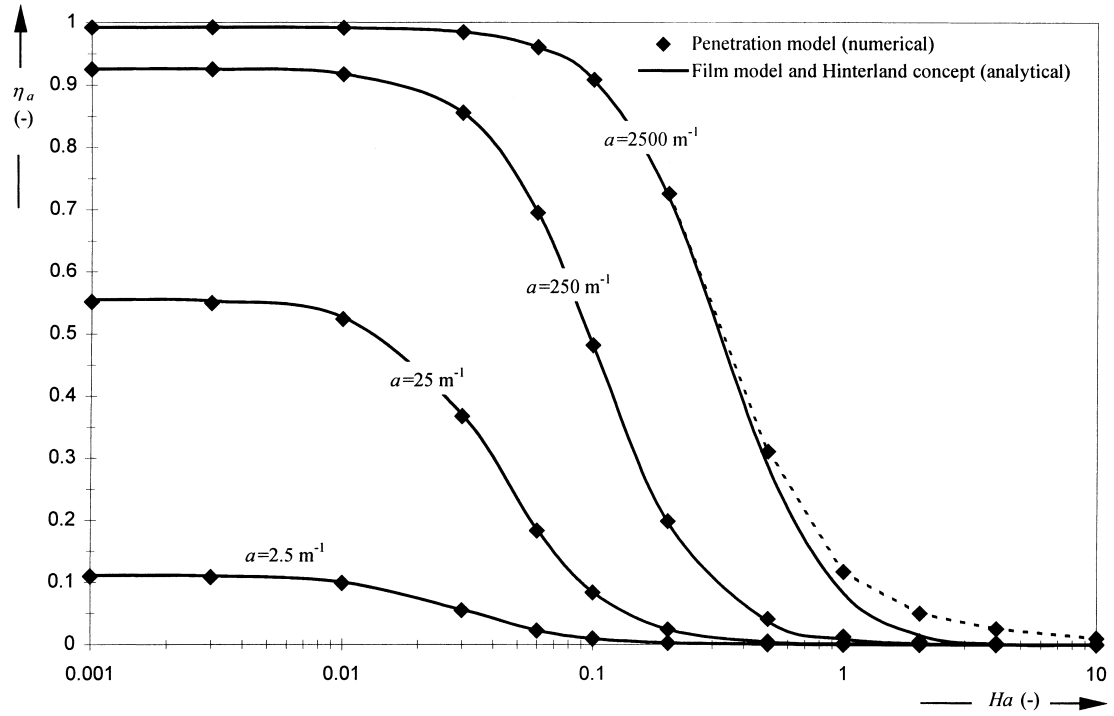

Fig. 9. Comparing analytical (Hinterland concept) and numerical results of saturation under steady state conditions of Case 3, varying the specific contact area from 2.5 to 2500 m^{-1}.

Table 5
Saturation under steady state conditions of Case 3 obtained with the presented model divided by the analytical solution of film model with Hinterland concept. A value of 1.0 means that both models give equal solutions

Ha	a=2.5 m^{-1}	a=25 m^{-1}	a=250 m^{-1}	a=2500 m^{-1}
0.001	1.0	1.0	1.0	1.0
0.003	1.0	1.0	1.0	1.0
0.01	1.0	1.0	1.0	1.0
0.03	1.0	1.0	1.0	1.0
0.06	1.0	1.0	1.0	1.0
0.1	1.0	1.0	1.0	1.0
0.2	1.0	1.0	1.0	1.0
0.5	1.1	1.1	1.1	1.1
1	1.4	1.4	1.4	1.4
2	3.6	3.6	3.6	3.6
4	27	27	27	27
10	∼11000	∼11000	∼11000	∼11000

5.3. Absorption and irreversible 1,1-reaction

For this case (see Table 6) an exact analytical solution is not available. van Krevelen and Hoftijzer [13] gave an approximate analytical solution method. The essence of their method is the approximation of the concentration profile of component B by a constant $[B]_1$ all over the reaction zone, so that the reaction becomes essentially pseudo first-order.

For calculation of the enhancement factor their method requires the maximum enhancement factor, which for the penetration model is at least in good approximation given by

$$E_{a\infty} \cong \left(1 + \frac{D_b[B]_{bulk}}{\gamma_b D_a [A]_i}\right)\sqrt{\frac{D_a}{D_b}} \quad (31)$$

For situations where the diffusion coefficients D_a and D_b are the same the van Krevelen and Hoftijzer method gives very good results (Table 7). The conditions for this case were chosen so that the enhancement factor of the van Krevelen and Hoftijzer method equals $E_{a\infty}$ so that they are easy to verify.

However, if the diffusion coefficients of components A and B are different, the deviations increase significantly

Table 6
Parameters used in Cases 4 and 5

Case	A(g) → A(l), A(l)+B(l) → P(l); R_a=$k_{R,1,1}$[A][B]
$k_{R,1,1}$	250 000 (Ha≫2) (Case 4)
	$2.5\times10^{-6} \le k_{R,1,1} \le 2.5\times10^{12}$ (Case 5)
$[A]_{g,in}$	1 mol m^{-3}
$[B]_{l,in}$	1 mol m^{-3}
k_l	5×10^{-5} m s^{-1}
k_g	100 m s^{-1} (no gas resistance)
D_a	10^{-9} m^2 s^{-1}
$D_{b,p}$	10^{-9} or 5×10^{-9} m^2 s^{-1}
m_a	$1 \le m \le 3$ (Case 4)
	m=0.5 (Case 5)
V_R	10 m^3
ε_g	0.5
a	100 m^2 m^{-3}
$\Phi_{g,in/out}$	0.01 m^3 s^{-1}
$\Phi_{l,in/out}$	0.01 m^3 s^{-1}
θ	0.51 s

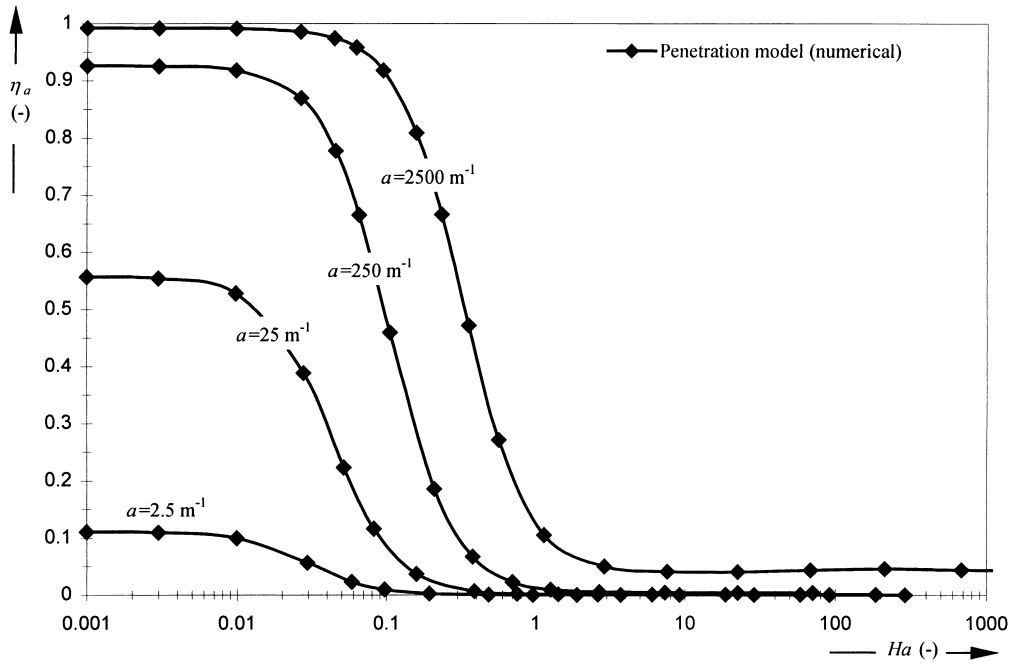

Fig. 10. Numerical results of saturation under steady state conditions of Case 5, varying the specific contact area from 2.5 to 2500 m^{-1}.

Table 7
Comparing approximate analytical solution of Eq. (31) with numerical results (160 gridpoints) for Case 4 with $D_a=D_b=10^{-9}\,m^2\,s^{-1}$

m_a	Eq. (31)	$E_{a,num}$
1.0	2.000	2.002
2.0	1.500	1.502
3.0	1.333	1.335

(Table 8). This is probably caused by a wrong approximation of the infinite enhancement factor (Eq. (31)). For a case with $[B]_{bulk}/\gamma_b[A]_i$ not much larger than one, Lightfoot [26] suggests the following equation:

$$E_{a\infty} \cong 1 + \frac{D_b[B]_{bulk}}{\gamma_b D_a[A]_i}\sqrt{\frac{D_a}{D_b}} \quad (32)$$

which is also given in Table 8.

From Table 8 it can be concluded that large discrepancies exist between Eq. (31) and (32) and the exact numerical solution under certain conditions.

Additional simulations were performed with Case 5, which differs slightly from Case 4, varying the specific contact area a from 2.5 to 2500 m^{-1}. The simulation conditions are given in Table 6 and the steady state results are shown in Fig. 10.

Table 8
Comparing approximate analytical solutions of Eqs. (31) and (32) with numerical results (160 gridpoints) for Case 4 with $D_a=10^{-9}\,m^2\,s^{-1}$ and $D_b=5\times10^{-9}\,m^2\,s^{-1}$

m_a	Eq. (31)	$E_{a,num}$	Eq. (32)
1.0	2.681	2.892	3.232
2.0	1.565	1.871	2.117
3.0	1.193	1.554	1.745

Table 9
Saturation under steady state conditions of Case 5 obtained with the presented model for large Hatta numbers (Ha>2.0)

a=2.5 m^{-1}	a=25 m^{-1}	a=250 m^{-1}	a=2500 m^{-1}
0.00004	0.0004	0.004	0.04

For a specific contact area of 2.5, 25 and 250 m^{-1} the solution is at first glance as expected: at low Hatta numbers the saturation approaches a maximum and at high Hatta numbers the saturation approaches zero. This was explained in Section 4.4, conclusions 5 and 6. However, at a specific contact area of 2500 m^{-1}, the saturation clearly does not approach zero (Fig. 10), even at very high Hatta numbers (Ha=1000). The penetration theory predicts still substantial concentrations of species A present in the liquid phase for Ha > 2.0. A saturation was found of 0.04 (4%) for Ha > 7.0, independent of the Hatta number (7.0<Ha<70 000). The Hinterland ratio Al equals 10 for Case 5 at a=2500 m^{-1}, which means that the process is still characterised by a significant liquid bulk. The ratio of the maximum conversion in the liquid bulk to the maximum transport through the film, $(Al-1)Ha^2$, is much larger than 1 for Ha > 7.0 ($(Al-1)Ha^2$=441 at Ha=7.0).

More detailed analysis of the cases for a specific contact area of 2.5, 25 and 250 m^{-1} shows that here also the saturation does not converge to zero at high Hatta numbers. This is not visible from Fig. 10 because of the scale of the y-axis, but from Table 9 it is clear that there is a limit slightly

above zero for all cases. The reason for the saturation not approaching zero is that the penetration model assumes liquid elements that are mixed up with the liquid bulk after each contact period. Therefore, the species present inside the liquid element are considered part of the liquid phase.

We are aware that Ha=70 000 are not usually found in process industry. We only used these extreme numbers to show that even at these extremely high Hatta numbers, the saturation does not converge to zero. In fact we show that, at a realistic Ha=7, the same saturation is found as for Ha=70 000 (Fig. 10). This is true, no matter what the value of the specific contact area is (Table 9).

Why does for a 1,0-reaction (Section 5.2, Fig. 9) the saturation of the liquid phase with species A converge to zero with increasing Hatta number, while for a 1,1-reaction (Fig. 10) the saturation converges to a certain constant slightly above zero, even if the Hatta number is increased up to 70 000? This can be explained by studying the concentration profiles of the liquid element at the end of the contact period.

The concentration profiles of the 1,0-reaction at various Hatta numbers are shown in Fig. 11. From this figure it is clear that the amount of species present in the liquid element (the area under the graph) converges to zero with increasing Hatta number and therefore the liquid phase saturation will also converge to zero.

The concentration profiles of the 1,1-reaction at various Hatta numbers are shown in Fig. 12. From this figure it is clear that the amount of species A present in the liquid element (the area under the graph of species A) does not converge to zero with increasing Hatta number. For this specific case, the area under the graph does not change for Hatta numbers larger than about 7. Therefore the liquid phase saturation does converge to a constant value, corresponding to the amount of species A marked by the grey triangle in Fig. 12. The size and shape of this triangle is the same for all Ha>7 for this case.

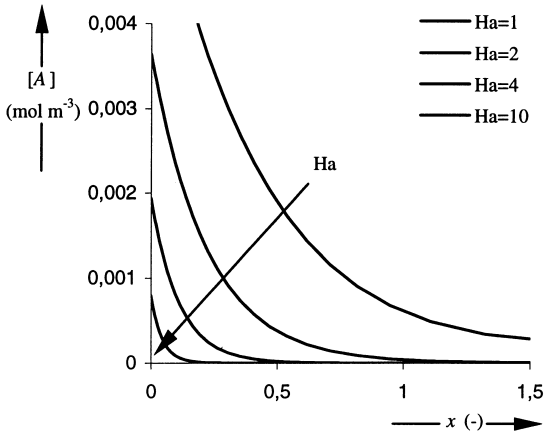

Fig. 11. Concentration profiles in the liquid element at the end of a contact period for Case 3 at steady state conditions and a=2500 m^{-1}. The reaction rate constant was varied to obtain Hatta numbers of 1, 2, 4 and 10.

The reason that for a 1,0-reaction the area under the concentration profile converges to zero, while for a 1,1-reaction this is not the case, is explained below:

1. For a 1,0-reaction, species A is the only required reactant and increasing the Hatta number by increasing the reaction rate constant will under all circumstances increase the conversion of species A inside the liquid element and lower the concentration of species A. At large enough rate constants the concentration of species A will converge to zero.
2. For a 1,1-reaction, species A reacts with species B. This means that component B is required to convert component A into the products. Increasing the Hatta number by increasing the reaction rate constant will initially increase the conversion of species A. However, above a certain reaction rate the supply of component B coming from the liquid bulk becomes limiting — a so-called instantaneous reaction — and further increase of the reaction rate does not increase the conversion. At large enough rate constants the concentration of species A will converge to a constant value larger than zero. From the concentration profiles shown in Fig. 12 it is obvious that for Case 5 at Ha>7 the supply of component B for the liquid phase becomes limiting (for x<0.4 component B is not available and the reaction is instantaneous).

5.4. Instantaneous reaction without enhancement

A special case occurs for instantaneous reactions (Ha≫2) without chemical enhancement of mass transfer (E_a=1). Case 4 (see Table 6) is an example of such a case if a=2500 m^{-1}, D_b=5×10^{-9} m^2 s^{-1} and m=3.0. For these conditions the enhancement factor equals the maximum enhancement factor $E_{a\infty}$=1.09≈1.

The concentration profile in the liquid element for this case is shown in Fig. 13. The penetration theory does not have any difficulties with calculating and processing this profile. The corresponding profile for the stagnant film model is shown schematically in Fig. 14. From this figure it is clear that the concentration profile of the film model has a discontinuity at x=δ for this specific case. This discontinuity may lead to serious difficulties when applying the stagnant film model for such a case.

5.5. Equilibrium reaction

Case 6 in Table 10 defines a case with an equilibrium reaction. The equilibrium constant is 10 and varying the reaction rate constant of the forward reaction varies the Hatta number (based on the forward reaction) from 0.001 to 100. The steady state saturation is shown in Fig. 15 as a function of Hatta number and specific contact area. The model has no difficulties handling the area where the liquid phase is not at equilibrium (Ha<1.5).

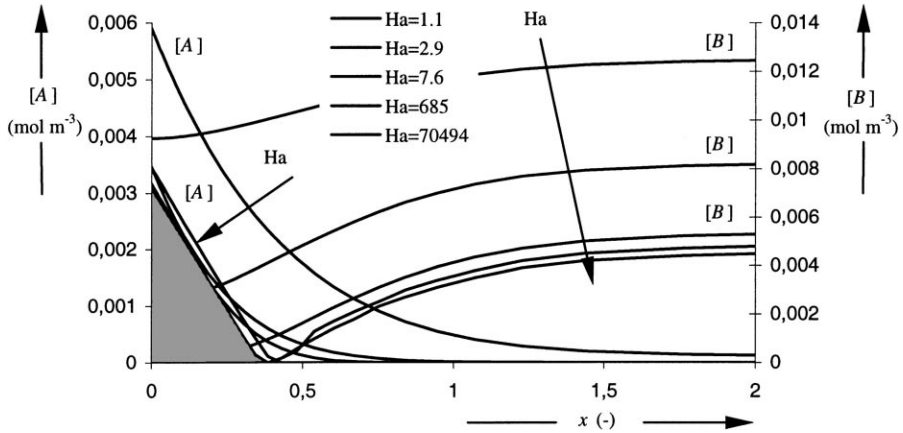

Fig. 12. Concentration profiles in the liquid element at the end of a contact period for Case 5 at steady state conditions and a=2500 m^{-1}. The reaction rate constant was varied to obtain Hatta numbers of 1, 3, 8, 685 and 70 494.

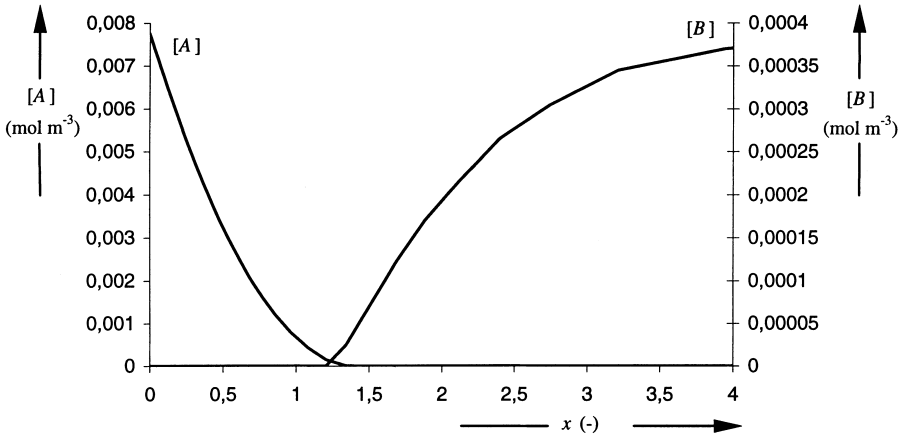

Fig. 13. Concentration profiles in the liquid element at the end of a contact period for Case 4 at steady state conditions and a=2500 m^{-1}, D_b=5×10^{-9} m^2 s^{-1} and m=3.0 (instantaneous reaction without enhancement).

Comparing Fig. 15 with Fig. 10 shows the influence of the backward reaction. The backward reaction decreases the net conversion of species A in the liquid phase and thereby increases the saturation. For very low Hatta numbers the saturation converges to the same limits in both Figs. 10 and 15. At large Hatta numbers the influence of the backward reaction forces the saturation of species A to increase.

Table 10
Parameters used in Case 6

Case	A(g)→A(l), A(l) + B(l)⇄C(l) + D(l), R_a=$k_{R,1,1}$[A][B]−$k_{R,-1,-1}$[C][D]
$k_{R,1,1}$	2.5×10^{-6}≤$k_{R,1}$≤250 000 m^6 mol^{-2} s^{-1}
K_{eq}=$k_{R,1,1}$/$k_{R,-1,-1}$	10
$[A]_g^0$ (initial state)	1 mol m^{-3}
$[B]_l^0$ initial state)	1 mol m^{-3}
$[A, C, D]_l^0$(initial state)	0 mol m^{-3}
k_l	5×10^{-5} m s^{-1}
k_g	100 m s^{-1} (no gas resistance)
D_i	10^{-9} m^2 s^{-1}
m_a	0.5
V_R	10 m^3
ε_g	0.5
a	2.5, 25, 250 and 2500 m^2 m^{-3}
$\Phi_{g,in/out}$	0.01 m^3 s^{-1}
$\Phi_{l,in/out}$	0.01 m^3 s^{-1}
θ	0.51 s

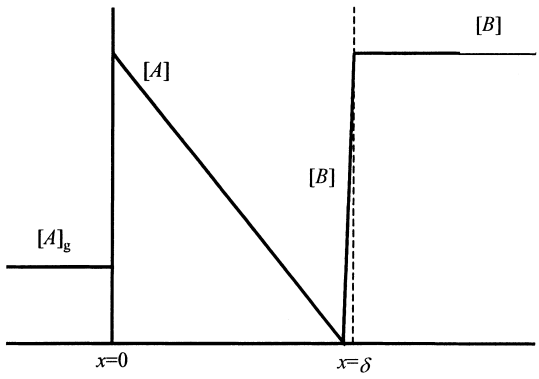

Fig. 14. Schematic concentration profile for the stagnant film model, corresponding to the profile for the penetration model presented in Fig. 13 (instantaneous reaction without enhancement).

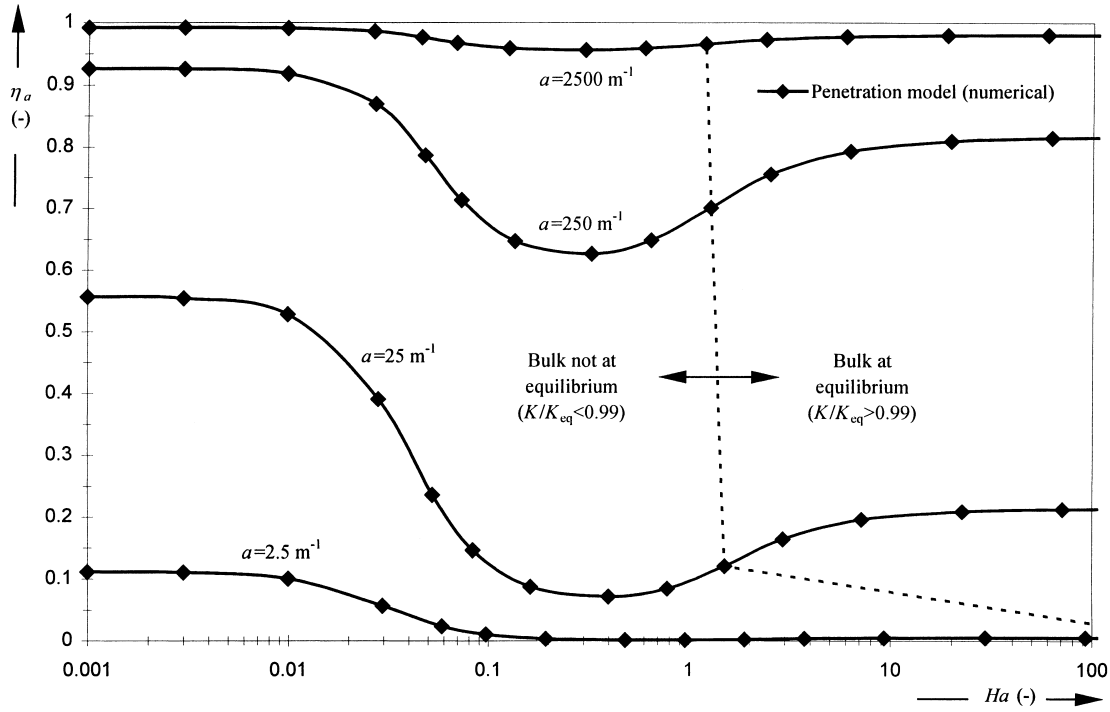

Fig. 15. Numerical results of saturation under steady state conditions of Case 6, varying the specific contact area from 2.5 to 2500 m^{-1}.

6. Conclusions

The main conclusion is that the dynamic behaviour of ideally stirred gas–liquid reactors can be simulated successfully over a wide range of conditions with the numerical solution method presented in this study. From comparison of the numerical results with analytical solutions it was concluded that the errors can be neglected.

Contrary to many other numerical and analytical models the present model can be used over a wide range of conditions. The model is suitable for the entire range of Hatta numbers for both reversible and irreversible reactions.

Multiple (in)dependent reactions, even with more than one gas phase component, can be implemented in the model as well, by extending the number of components and the kinetic rate expression. The model can also be used for simulation of (semi-)batch reactors.

Since the Hinterland concept [3] requires a constant mass transfer flux from the liquid film or element to the liquid bulk phase, the Hinterland concept is not directly applicable to the penetration models. The model presented in this study successfully uses a different approach to implement the simultaneous solution of the Higbie penetration and the dynamic gas–liquid macro model.

Under some circumstances substantial differences exist between the exact numerical and existing approximate results. For specific cases substantial differences can exist between the results obtained using the stagnant film model with Hinterland concept and the presented implementation of the Higbie penetration model.

The numerical model presented in this study is especially useful for complex systems for which no analytical solutions exist and for which the stagnant film model in not accurate.

7. Nomenclature

a	specific surface area ($m^2\,m^{-3}$)
A	component A
Al	Hinterland ratio (defined by $\varepsilon_l/\delta a$)
B	component B
C	component C
D	component D
$D_{\text{subscript}}$	diffusivity ($m^2\,s^{-1}$)
$E_{\text{subscript}}$	enhancement factor
$E_{\text{subscript}\infty}$	enhancement factor for instantaneous reaction
Ha	Hatta number defined by $(k_{R,m,n,p,q}[A]^{m-1}[B]^n[C]^p[D]^q D_a)^{0.5}/k_l$
$J_{\text{subscript}}$	molar flux ($mol\,m^{-2}\,s^{-1}$)
k_g	gas phase mass transfer coefficient ($m\,s^{-1}$)
k_l	liquid phase mass transfer coefficient ($m\,s^{-1}$)
k_{ov}	overall mass transfer coefficient ($m\,s^{-1}$)
$k_{R,\text{subscript}}$	reaction rate constant ($m^{3(m+n+p+q-1)}\,mol^{-(m+n+p+q-1)}\,s^{-1}$ or $m^{3(r+s+t+v-1)}\,mol^{-(r+s+t+v-1)}\,s^{-1}$)
m	reaction order
$m_{\text{subscript}}$	gas–liquid partition coefficient
n	reaction order

N	counter with start value 1 at t=0
$N_{\text{subscript}}$	number of moles (mol)
p	reaction order
q	reaction order
r	reaction order
$R_{\text{subscript}}$	reaction rate (mol m^{-3} s^{-1})
s	probability of replacement according to surface renewal model
s	reaction order
t	reaction order
t	simulation time variable (s)
v	reaction order
V_R	reactor volume (m^3)
x	place variable (m)
$x_{\text{dimensionless}}$	place variable defined as $x/\sqrt{4D_a\theta}$
[]	concentration (mol m^{-3})
$[]_{\text{subscript}}$	concentration (mol m^{-3})

Greek letters

δ	film thickness according to film model (m)
δ_p	assumed thickness of liquid element (m)
ε_g	gas phase hold-up
ε_l	liquid phase hold-up
$\gamma_{\text{subscript}}$	stoichiometry number
η	degree of utilisation
$\eta_{\text{subscript}}$	degree of saturation
θ	contact time according to penetration model (defined by $4D_a/\pi k_l^2$) (s)
τ_g	gas phase residence time (s)
τ_l	liquid phase residence time (s)
$\xi_{\text{subscript}}$	absolute conversion (mol)
Φ_g	gas phase volume flow rate (m^3 s^{-1})
Φ_l	liquid phase volume flow rate (m^3 s^{-1})

Subscripts

a	component A
an	analytical solution
b	component B
bulk	at bulk conditions
c	component C
d	component D
elem	at liquid element conditions
film	film model
g	gas phase
i	interface
i	species *i*
in	at inlet conditions
l	liquid phase
num	numerical solution
out	at outlet conditions
p	penetration element
pen	penetration model
sat	at saturation conditions

Superscripts

0	initial value
j	time level

Acknowledgements

These investigations were supported by DSM Research Geleen.

References

[1] L.K. Doraiswamy, M.M. Sharma, Heterogeneous Reactions, Vol. 2, Wiley, New York, 1984.
[2] S. Hatta, Tech. Rep. Tohoku Imp. Univ. 10 (1932) 119.
[3] K.R. Westerterp, W.P.M. van Swaaij, A.A.C.M. Beenackers, Chemical Reactor Design and Operation, Wiley, New York, 1990.
[4] W.G. Whitman, Preliminary experimental confirmation of the two-film theory of gas absorption, Chem. Metall. Eng. 29 (1923) 146–148.
[5] R. Higbie, The rate of absorption of a pure gas into a still liquid during short periods of exposure, Trans. Am. Inst. Chem. Eng. 35 (1935) 36–60.
[6] P.V. Danckwerts, Significance of liquid-film coefficients in gas absorption, Ind. Eng. Chem. 43 (1951) 1460–1467.
[7] W.E. Dobbins, in: M.L. McCable, W.W. Eckenfelder (Eds.), Biological Treatment of Sewage and Industrial Wastes, Part 2-1, Reinhold, New York, 1956.
[8] H.L. Toor, J.M. Marchello, Film-penetration model for mass transfer and heat transfer, AIChE J. 4 (1958) 97–101.
[9] T.K. Sherwood, R.L. Pigford, Absorption and Extraction, McGraw-Hill, New York, 1952, p. 332.
[10] P.V. Danckwerts, A.M. Kennedy, Kinetics of liquid-film process in gas absorption. Part 1: Models of the absorption process, Trans. Inst. Chem. Eng. 32 (1954) 49–53.
[11] D.R. Olander, Simultaneous mass transfer and equilibrium chemical reaction, AIChE J. 6 (1960) 233–239.
[12] C.-J. Huang, C.-H. Kuo, Mathematical models for mass transfer accompanied by reversible chemical reaction, AIChE J. 11 (1965) 901–910.
[13] D.W. van Krevelen, P.J. Hoftijzer, Kinetics of gas–liquid reactions. Part 1: General theory, Rec. Trav. Chim. 67 (1948) 563–568.
[14] K. Onda, E. Sada, T. Kobayashi, M. Fujine, Gas absorption accompanied with complex chemical reactions — I. Reversible chemical reactions, Chem. Eng. Sci. 25 (1970) 753–760.
[15] W.J. DeCoursey, Enhancement factors for gas absorption with reversible reaction, Chem. Eng. Sci. 37 (1982) 1483–1489.
[16] H. Hikita, S. Asai, A. Yano, H. Nose, Kinetics of absorption of carbon dioxide into aqueous sodium sulfite solutions, AIChE J. 28 (1982) 1009–1015.
[17] L. Landau, Desorption with a chemical reaction, Chem. Eng. Sci. 47 (1992) 1601–1606.
[18] S.J. Parulekar, N.A. Saidina Amin, Complex gas–liquid reactions: feedback from bulk liquid to liquid-side film, Chem. Eng. Sci. 51 (1996) 2079–2088.
[19] J.J. Romanainen, T. Salmi, Numerical strategies in solving gas–liquid reactor models — 1. Stagnant films and a steady state CSTR, Comput. Chem. Eng. 15 (1991) 769–781.
[20] J.J. Romanainen, T. Salmi, Numerical strategies in solving gas–liquid reactor models — 2. Transient films and dynamic tank reactors, Comput. Chem. Eng. 15 (1991) 783–795.
[21] G.F. Versteeg, P.M.M. Blauwhoff, W.P.M. van Swaaij, The effect of diffusivity on gas–liquid mass transfer in stirred vessels. Experiments at atmospheric and elevated pressures, Chem. Eng. Sci. 42 (1987) 1103–1119.

[22] E.P. van Elk, P.C. Borman, J.A.M. Kuipers, G.F. Versteeg, Modelling of gas–liquid reactors — stability and dynamic behaviour of gas–liquid mass transfer accompanied by irreversible reaction, Chem. Eng. Sci. 54 (1999) 4869–4879.
[23] G.F. Versteeg, J.A.M. Kuipers, F.P.H. van Beckum, W.P.M. van Swaaij, Mass transfer with complex reversible chemical reactions — I. Single reversible chemical reaction, Chem. Eng. Sci. 44 (1989) 2295–2310.
[24] W.P.M. van Swaaij, G.F. Versteeg, Mass transfer accompanied with complex reversible chemical reactions in gas–liquid systems: an overview, Chem. Eng. Sci. 47 (1992) 3181–3195.
[25] G.A. Baker, T.A. Oliphant, An implicit, numerical method for solving the two-dimensional heat equation, Quart. Appl. Math. 17 (1960) 361–373.
[26] E.N. Leightfoot, Approximate expressions for predicting the effect of fast second-order chemical reaction on interphase mass-transfer rates, Chem. Eng. Sci. 17 (1962) 1007–1011.